Original Article

Journal of Intelligent Material Systems and Structures

Journal of Intelligent Material Systems and Structures
1–14

DOI: 10.1177/1045389X15585897
jim.sagepub.com
SAGE

Ultrasonically powered piezoelectric generators for bio-implantable sensors: Plate versus diaphragm

David B Christensen and Shad Roundy

Abstract

This article is a comparative study of the design spaces of two bio-implantable acoustically excited generator architectures: the bulk-mode piezoelectric plate (plate) and the flexure-mode unimorph piezoelectric diaphragm (diaphragm). The acoustic to electrical power transducers, or generators, are part of an acoustic, or ultrasonic, power transfer system for implantable sensors and medical devices such as glucose monitors, metabolic monitors, and drug delivery systems. Scalable network equivalent models are presented and used to predict that for sub-millimeter size devices, the diaphragm architecture generates more power than the plate architecture and is less sensitive to absorption power losses with increased implant depth. The models are compared to the experimental data from centimeter-size devices. This article will present and compare the power loss mechanisms and total power generated for each of the architectures as a function of diameter, aspect ratio, and implanted depth.

Keywords

Piezoelectric transducer, implantable sensors, acoustic energy harvesting, ultrasonic generator, wireless power transfer, acoustic radiation loss, piezoelectric micromachined ultrasonic transducer, ultrasound equivalent circuit model, bulk-mode transducer

Introduction

Interest in and realization of millimeter scale bio-implantable devices has increased with advances in power electronics, sensing, complementary metal-oxide-semiconductor (CMOS), and communications technology. Bio-implantable devices are small devices that are implanted in the body in order to perform a diagnostic or therapeutic function. Such functions range from glucose sensing to drug delivery. For example, an implantable glucose sensor will allow diabetics to obtain real-time, accurate glucose readings without pricking their finger thus enabling better management of the disease. Various methods have been published to power bio-implantable devices both on-board (from inside the body) and wirelessly (from outside the body). On-board powering methods include batteries and biological fuel cells. Wireless methods include magnetic, near-field inductive, and acoustic power transfer. Two piezoelectric generator architectures that may be employed for acoustic power transfer are the bulk-mode circular plate (plate) and the flexure-mode unimorph diaphragm (diaphragm) shown in Figure 1.

The plate is a circular piezoelectric disk that is rigidly fixed/clamped around its circumference. It is poled (3-3 axis) perpendicular to the face of the plate. The front face is in contact with tissue and the back face is open to a vacuum. Its aspect ratio ($=2a/h_p$) is constrained to be no less than 1 and no greater than 10. An aspect ratio less than 1 results in the plate's thickness being larger than its diameter which makes diameter a poor measure of overall implant size. An aspect ratio greater than 10 introduces bending (strain in 3-1 direction) as the dominant strain mode and thus requires a different model. The housing is modeled as rigid, having no other dynamics than to impose a fixed/clamped condition about the circumference of the plate.

The diaphragm is a circular piezoelectric disk fixed to the back side of a larger circular non-piezoelectric shim. The piezoelectric disk is poled perpendicular to its face. The shim is fixed/clamped around its circumference with its front face in contact with tissue and its

Department of Mechanical Engineering, University of Utah, Salt Lake City, UT, USA

Corresponding author:
David B Christensen, Department of Mechanical Engineering, University of Utah, Salt Lake City, UT 84112, USA.
Email: dave.christensen@utah.edu

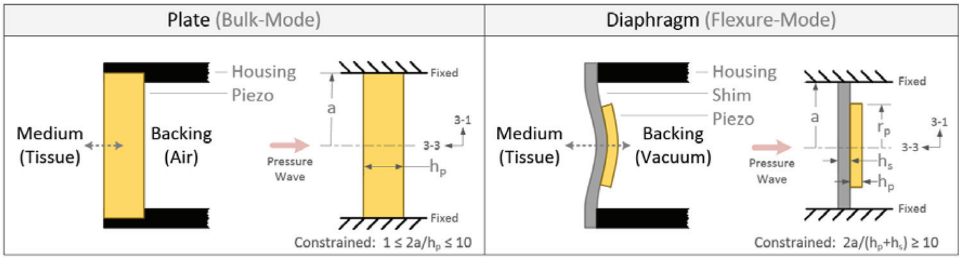

Figure 1. Side-view cross section of the plate (left) and diaphragm (right) with relevant dimensions, boundary conditions, and poling directions. Note that in the front view, both the plate and diaphragm architectures are circular.

Table 1. Published works that provide simulation and/or experimental results for bio-implantable sensors using wireless acoustic power transfer.

Year	Article	Architecture	Diameter	Frequency	Depth	Medium
Devices						
2001	Kawanabe et al. (2001)	Plate	30 mm	1 MHz	7–100 mm	Water, goat tissue
2007	Arra et al. (2007)	Plate	25 mm	840 kHz	5–105 mm	Water
2009	Ozeri and Shmilovitz (2010)	Plate	15 mm	673 KHz	40 mm	Pig muscle
2011	Shigeta et al. (2011)	Plate	44 mm	1.2 MHz	–	Water
Simulations						
2010	Denisov and Yeatman (2010)	Plate	2–10 mm	$\leqslant$1 MHz	10–100 mm	Tissue
2012	Sanni et al. (2012)	Plate	10 mm	200 kHz	$\leqslant$70 mm	Tissue
2013	Seo et al. (2013)[a]	Plate	10–100 μm	10 MHz	2 mm	Brain tissue

[a]White paper published to arXiv. No experimental data have been published on this work.

back face open to a vacuum. Its aspect ratio ($= 2a/(h_s + h_p)$) is constrained to be greater than or equal to 10 so that the strain in the piezoelectric disk is dominant in the 3-1 direction (bending). The housing is modeled as rigid, having no other dynamics than to impose a fixed/clamped condition about the circumference of the shim.

The plate is widely used in diagnostic and therapeutic ultrasound and seems the natural candidate for high acoustic to electrical power generation at the millimeter scale because of its high acoustic power output as a transmitter. On the other hand, the diaphragm can easily be overlooked for acoustic to electrical power generation for two reasons. First, it operates in the 3-1 mode which has a lower coupling coefficient than the 3-3 mode of the plate. Second, diaphragms use significantly less piezoelectric material than plates of the same diameter and are thus usually outperformed by plates in terms of acoustic to electrical power generation. However, the diaphragm has a strength that is particularly useful for bio-implantable power applications: it can operate at much lower frequencies than the plate (meaning less signal attenuation and tissue heating). It should be noted that in Figure 1 the piezoelectric layer does not extend over the entire diaphragm. In some other common diaphragm, or piezoelectric micromachined ultrasonic transducer (PMUT), designs, the piezoelectric layer does extend over the entire diaphragm. The results presented here do not substantially change if the piezoelectric layer extends over the entire diaphragm.

The literature focusing on the plate architecture as a means of power generation in bio-implantable devices is not new. Table 1 gives a sampling of works as far back as 2001. Kawanabe et al. (2001) and Arra et al. (2007) explored plate-to-plate transmission separated by tissue. Ozeri and Shmilovitz (2010) and Shigeta et al. (2011) took the analysis further by adding a quarter wavelength matching layer to the plate to reduce pressure reflections at the generator surface. Denisov and Yeatman (2010) performed a comparison between near-field inductive and acoustic power transfer concluding that near-field inductive power transfer is more efficient for larger devices with shallower tissue depths while acoustic power transfer is more efficient for smaller devices with deeper tissue depths. Sanni et al. (2012) and Seo et al. (2013) proposed hybrid systems where a larger inductive power transfer system transmitted power through skin and/or bone to a smaller in vivo acoustic plate-to-plate system. It is notable that the plate diameters of interest are, for the most part, decreasing with time.

The literature focusing on the diaphragm architecture as a means of power generation in bio-implantable devices at the millimeter scale is not as prevalent as the plate. In 2001, Ramsay and Clark (2001) performed

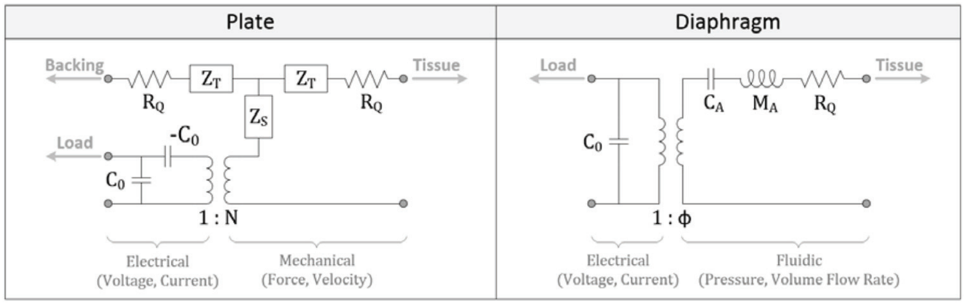

Figure 2. Equivalent circuit models for the plate (left) and diaphragm (right). The gray arrows with labels indicate external components that attach to each port. The labels beneath the circuit indicate the domain with their associated power states (effort, flow).

a feasibility study concluding that diaphragms could harvest enough power from pulsing blood vessels to continuously power a μW microelectromechanical systems (MEMS) device. Further modeling and experimental validation of the more complicated diaphragm system has since then been made (Kim et al., 2003; Mo et al., 2010a, 2010b; Prasad et al., 2006; Smyth, 2012) for applications ranging from wearable energy harvesters and flow control devices to diagnostic imaging where it is referred to as a PMUT, the piezoelectric counterpart to the capacitive micromachined ultrasonic transducer (CMUT). The modeling and use of the diaphragm in in vivo powering applications is not new, but powering the in vivo diaphragm via wireless acoustic power transfer at ultrasonic frequencies is. The merit of this work is that it provides an analysis on the acoustically powered diaphragm structure as a millimeter scale generator implanted in the body and compares its performance with the plate architecture.

The remainder of this article is organized as follows. Lumped parameter models of the plate and diaphragm are presented. A detailed discussion of loss mechanisms and the models for those mechanisms is follows. Experimental validation for the lumped parameter and loss models is presented at relatively large (i.e. 1 cm diameter devices) size scales. The models are then used to study acoustic to electrical power generation as generator sizes are scaled down to 100 μm in diameter over implant depths from 1 to 5 cm.

Modeling

Acoustic transducers are often modeled with lumped parameter circuit models (Prasad et al., 2006; Sherrit et al., 1999). Equivalent circuit models are useful in that they can be simulated rapidly and used to quickly optimize a design. The circuit components used to model the plate and diaphragm are given in Figure 2. The plate model employed is Mason's model which is equivalent to the well-known Krimholtz, Leedom, and Matthae (KLM) (Sherrit et al., 1999). The diaphragm model used was proposed by Prasad et al. (2006). Prasad's model is derived from composite plate theory and is supported by experimental validation. We have employed these basic circuit models in conjunction with analytical models for acoustic radiation loss and viscous drag. These losses take the form of the resistor R_Q and enable proper scaling of simulation data without having to gather empirical loss measurements at each transducer size. These losses are discussed further in section "Damping" of this article. It is important to note that in the prior published works, the transmitter dynamics have played an important role in the power and efficiency results of the generator (Sherrit et al., 2005). In this work, the transmitter dynamics are only modeled in section "Experimental setup and model validation" of this article. In all other simulations, the transmitter is replaced by a 7200 W/m^2 intensity source (see Figure 3), the spatial-peak-temporal-average intensity limit specified by the US Food and Drug Administration (FDA) (Guidance for Industry and FDA Staff Information for Manufacturers Seeking Marketing Clearance of Diagnostic Ultrasound Systems and Transducers, 2008).

Power losses

A primary design goal for any power generation system is to minimize power losses. The dominant power losses for an ultrasonically powered implant are due to beam divergence, tissue absorption, pressure wave reflection, transducer damping, piezoelectric coupling, power electronics, and electrical load impedance mismatch. A visual representation of these losses and their implementation in the scaling simulation model are shown in Figure 3 followed by a brief discussion of each of the losses with insights to their dependence on diameter and aspect ratio. A list and explanation of variables and the properties of the piezoelectric material, shim, and tissue used to obtain the simulation results in the following paragraphs are given in Table 2.

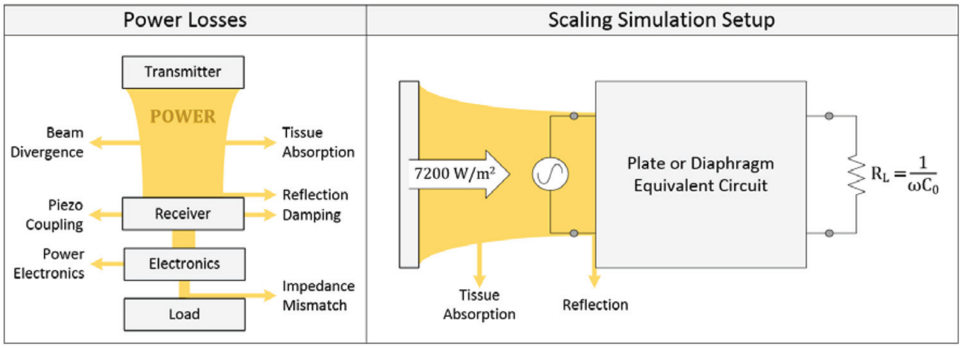

Figure 3. Left: sources of power loss between the transmitter's acoustic output and the load. Right: circuit model implementation for the scaling simulations in sections "Power losses" and "Generated power comparison" of this article. Note that the transmitter component is replaced by a source intensity and the pressure source on the transducer equivalent circuit represents the source pressure minus tissue absorption and reflection losses.

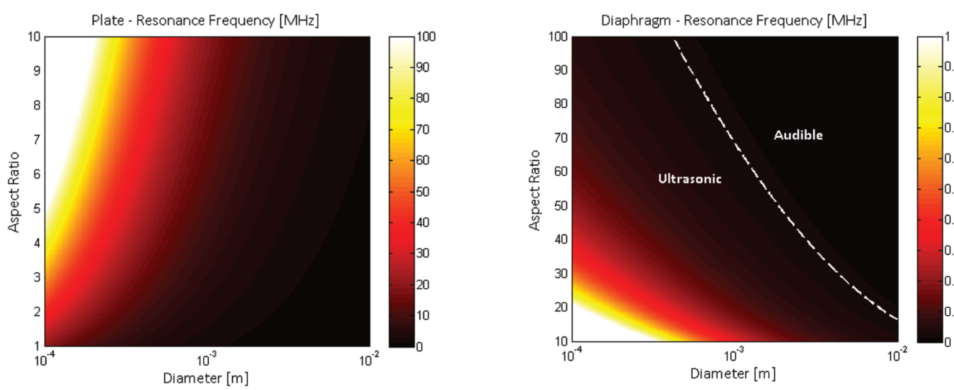

Figure 4. Resonance frequency of the plate (left) and diaphragm (right) implanted in muscle at various aspect ratios and diameters. The diaphragm graph is split by a white dotted line that represents the 20 kHz boundary between the audible and ultrasonic regions.

Beam divergence

Beam divergence is strongly dependent on the ratio of the transmitter diameter to the wavelength in the medium and thus will only be accounted for in section "Experimental setup and model validation" of this article. The acoustic beam radius, r_{beam}, for an unfocused circular plate is given in equation (1) and the associated power diverted is given in equation (2) (Christensen, 1988). Beam divergence for the diaphragm is approximated by setting the beam radius equal to the depth of the medium, d. Although the simulations in this article assume a focused beam (no power diverted), it is useful to note that a beam larger than the implant is likely desirable to facilitate supplying power to the implant

$$r_{beam} \approx \begin{cases} \text{Near Field} \rightarrow a \\ \text{Far Field} \rightarrow d\ \tan\left(\sin^{-1}\left(\frac{0.61c_t}{af}\right)\right) \end{cases} \quad (1)$$

$$\frac{P_{\text{diverted}}}{P_{\text{tranducer face}}} = 1 - \frac{a^2}{r_{beam}^2} \quad (2)$$

Tissue absorption

The power absorbed in tissue, or tissue heating, is given in equation (3) (Christensen, 1988) and is heavily dependent on acoustic frequency. As the acoustic frequency increases linearly, the acoustic power remaining, after traveling through the tissue, decreases exponentially. Therefore, to minimize power losses due to absorption, a generator should be designed with a low acoustic resonance frequency. The resonance frequency of the plate architecture, $f_{r,P}$, is given in equation (4). As the thickness of the plate decreases, its resonance frequency increases such that at millimeter thicknesses the resonance frequency is on the order of megahertz resulting in high tissue absorption. On the other hand, the resonance frequency of the diaphragm, $f_{r,D}$, given in equation (5) with the added virtual mass factor (AVMF) β given in equation (6) (Kozlovsky, 2009) and the viscosity scaling factor ξ given in equation (7), is on the order of kilohertz for similar sizes resulting in significantly lower tissue absorption than the plate. Figure 4 gives the resonance frequency of the

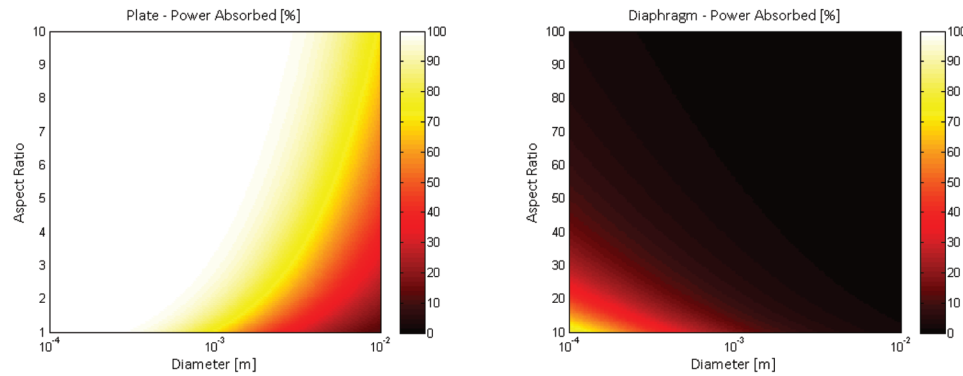

Figure 5. Percent of source power absorbed for the plate (left) and diaphragm (right) when implanted 2 cm into muscle. The power absorbed is dependent on the resonance frequency of the implanted generator.

plate and diaphragm architectures when surrounded by muscle for millimeter diameters. The resulting percent power lost through 2 cm of muscle is shown in Figure 5

$$\frac{P_{\text{absorbed}}}{P_{\text{source}}} = 1 - e^{-2\alpha_0 f^n d} \tag{3}$$

$$f_{r,P} = \frac{c_p}{2h_p} \tag{4}$$

$$f_{r,D} = \frac{1}{2\pi\sqrt{C_A M_A(1+\beta_D)}} \propto \frac{(h_s + h_p)}{a^2\sqrt{1+\beta_D}} \tag{5}$$

$$\beta_D = 0.6538\frac{\rho_t a}{\rho_D(h_s + h_p)}(1 + 1.082\xi) \tag{6}$$

$$\xi = \sqrt{\frac{v_t}{2\pi f_r a^2}} \tag{7}$$

Reflection

Reflection of acoustic pressure waves off the face of the implant receiver is due to acoustic impedance mismatch between the tissue and the receiver. The acoustic impedance for the plate in terms of equivalent circuit impedances (see Figure 2) is given in equation (8) and the acoustic impedance of the diaphragm is given in equation (9). Note that subscripts P and D refer to the plate and diaphragm, respectively (see Table 2 for a complete list of variables). The power reflected from the surface of the plate or diaphragm when implanted in tissue is given in equation (10) (Christensen, 1988). Figure 6 gives a visual representation of the percent power reflected from the surface of the plate and diaphragm when implanted in muscle and excited at the fundamental mechanical resonance frequency of the transducer (resonance frequencies shown in Figure 4) as a function of diameter and aspect ratio. The white dotted line represents zero reflection or the point where the acoustic impedance of the transducer and muscle match. From the figure, it is apparent that the acoustic impedance (and thus power reflected) for both the plate and diaphragm can be adjusted with aspect ratio such that reflection is minimized. However, as diameter decreases, the sensitivity of the acoustic impedance to changes in aspect ratio decreases

$$Z_P = \frac{\left(\frac{Z_T + R_{Q,P}}{2} + Z_S\right)}{\pi a^2} \tag{8}$$

$$Z_D = \pi a^2(Z_{C_A} + Z_{M_A} + R_{Q,D}) \tag{9}$$

$$\frac{P_{\text{reflected}}}{P_{\text{generator face}}} = R^2_{t\to P/D} = \left(\frac{Z_{P/D} - Z_t}{Z_{P/D} + Z_t}\right)^2 \tag{10}$$

where $Z_t = \rho_t c_t$.

An effective way to reduce reflections for plate transducers is to add a quarter wavelength matching layer between the transducer face and the medium. The matching layer ideally has an acoustic impedance equal to $\sqrt{Z_t Z_P}$ and reduces the transducer's quality factor in addition to reflection. In diagnostic ultrasound, the reduction in quality factor and reflection is a win–win situation. In power transfer, the reduction in quality factor is the trade-off to the reduction in reflection. Furthermore, for an implant with size limitations, the matching layer acts to reduce the available thickness of the piezoelectric material which results in a higher frequency transducer with higher absorption. Thus, for this study, matching layers will not be considered for the plate transducer.

Damping

At millimeter diameters, the damping contributors of most significance are acoustic radiation loss and viscous drag. For the plate architecture, acoustic radiation loss is a function of acoustic impedance only and is given in equation (11). Viscous drag on the plate, given in equation (13), was derived using a procedure similar to that in Kozlovsky (2009) and Lamb (1920) and is dependent on the aspect ratio and the viscosity scaling factor ξ. On the other hand, both the acoustic

Table 2. Left: properties of the piezoelectric material, shim, and mediums used in the scaling simulations. Right: description of variables used in the equations presented in this article.

Description	Variable	Muscle	Water	Units
Density	ρ	1070	1000	kg/m^3
Speed of sound	c	1566	1500	m/s
Kinematic viscosity	υ	0.15	0.001	m^2/s
Absorption coefficient	α_0	0.15	0.00025	Np/cm MHz
Frequency coefficient	n	1	1	–

Description	Variable	Piezo	Shim	Units
Density	ρ	7600	10,490	kg/m^3
Speed of sound	c	4080	3650	m/s
Young's modulus	Y_{31}	63	100	GPa
	Y_{33}	54		
Poisson's ratio	ν	0.32	0.32	–
Permittivity	ε	16.815		nF/m
Charge constant	d_{31}	−0.175		nm/V
	d_{33}	0.4		
Coupling coefficient	k_{31}	0.36		–
	k_t	0.45		
	k_{33}	0.72		

Variable	Description	Units	Notes
a	Transducer radius	m	See Figure 1
c	Speed of sound	m/s	
d	Implant depth in tissue	m	
f	Frequency	Hz	When used in $\alpha_0 f^n$, f is in MHz
h	Transducer thickness	m	No subscript refers to total thickness
I	Acoustic intensity	W/m^2	
n	Frequency coefficient	–	
P	Power	W	
Q	Quality factor	–	
r	Radius	m	
$R_{1\rightarrow2}$	Reflection coefficient	–	From medium 1 to medium 2
ν	Poisson's ratio	–	
Y	Young's modulus	Pa	
Z	Acoustic impedance	Rayl	Also used for impedances in Figure 2
α_0	Absorption coefficient	Np/cm MHz	
β	Added virtual mass factor	–	
ξ	Viscosity scaling factor	–	
ρ	Density	kg/m^3	
υ	Kinematic viscosity	m^2/s	

Variables not found in this table are defined in Figures 1 to 3. Subscripts attached to the described variables are *a*, *b*, *p*, *r*, *t*, *w*, *P*, and *D* meaning (a)ir, (b)acking, (p)iezo, (r)esonance, (t)issue, (w)ater, (P)late, and (D)iaphragm, respectively. Sources: Christensen(1988), Jacobitz et al. (2011), Fox et al. (2009), APC International, Ltd (2013), Engineering ToolBox (2015a), (2015b).

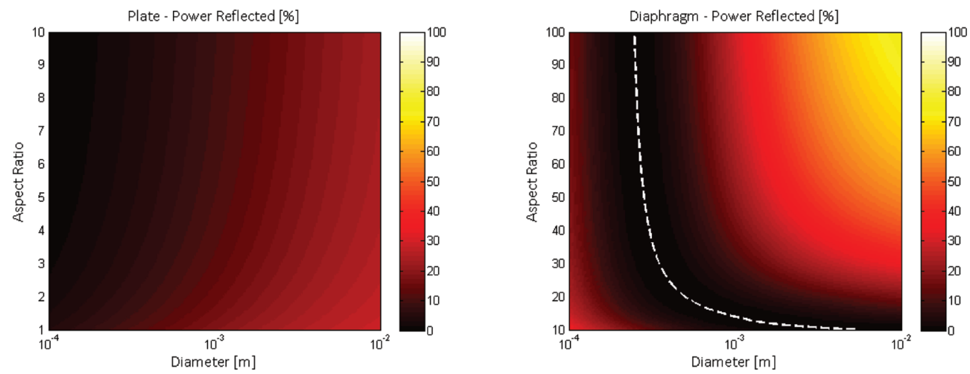

Figure 6. Percent power reflected from the plate (left) and the diaphragm (right) when implanted in muscle as a function of the aspect ratio and diameter. The white dotted line represents zero power reflected.

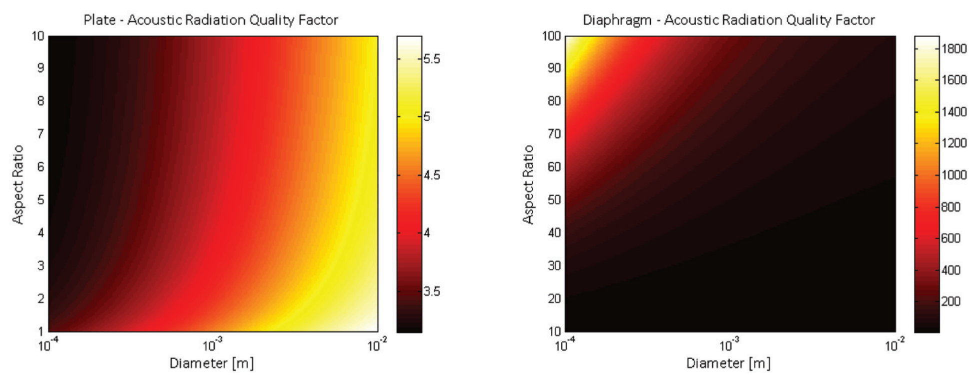

Figure 7. Acoustic radiation quality factor for the plate (left) and the diaphragm (right) when implanted in muscle as a function of diameter and aspect ratio.

radiation loss and viscous drag for the diaphragm are dependent on the AVMF β and the viscosity scaling factor ξ and are given in equations (12) and (14) (Olfatnia et al., 2011) respectively. The quality factor contributions to the plate and diaphragm are shown for acoustic radiation loss in Figure 7 and for viscous drag in Figure 8. As the figures clearly indicate, damping for the diaphragm is dominated by viscous losses while the damping contribution to the plate is similar for radiation and viscous losses. The combined quality factor as a function of diameter and aspect ratio is shown in Figure 9, which indicates a generally higher quality factor for the plate. To incorporate damping into the network models, the resistor R_Q is calculated for the plate in equation (15) and for the diaphragm in equation (16) where Q_{tot} includes the quality factor contributions from all sources of transducer-specific losses such as acoustic radiation loss, viscous drag, support loss, and crystal defects. Note that the quality factor contributions from acoustic radiation loss, viscous drag, and the manufacturer-specified "Mechanical Q" for the material are the only losses considered in this article. Also note that although a low-quality factor is desirable to achieve better axial resolution in diagnostic ultrasound, a high-quality factor is desirable to achieve more power to the load when the transducer is solely used for acoustic power transfer

$$Q_{rad,P} = \frac{\pi\left(1 + R^2_{P\to b} + R^2_{P\to b}R^2_{P\to t} + R^2_{P\to t}\right)}{Z_P\left(\frac{1}{Z_t}(1 + R_{P\to t})^2(1 + R^2_{P\to b}) + \frac{1}{Z_b}(1 + R_{P\to b})^2(1 + R^2_{P\to t})\right)} \tag{11}$$

$$Q_{rad,D} = 1.2\frac{\rho_D c_t}{\rho_t c_D}(1 + \beta_D)^{1.5}$$
$$\text{where} \quad c_D = \frac{c_p}{(1 - \nu_p^2)} \quad \text{and} \quad \rho_D = \frac{\rho_s h_s + \rho_p h_p}{h_s + h_p} \tag{12}$$

$$Q_{vis,P} = \frac{1}{\xi}\left(0.1911 + 0.2251\frac{\rho_p h_p}{\rho_t a}\right) + 0.1592 \tag{13}$$

$$Q_{vis,D} = \frac{0.95}{\xi}\left(\frac{1}{\beta_D} + 1\right) \tag{14}$$

$$R_{Q,P} = \frac{a^2 Y_{33}}{c_p Q_{tot}} \tag{15}$$

$$\text{where } Q_{tot} = ((1/Q_{rad}) + (1/Q_{vis}) + \ldots)^{-1}$$

$$R_{Q,D} = \frac{\sqrt{M_A/C_A}}{Q_{tot}} \tag{16}$$

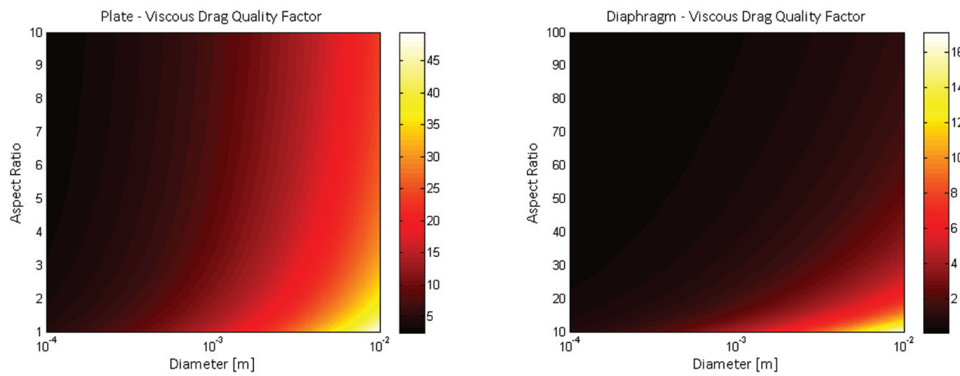

Figure 8. Viscous drag quality factor for the plate (left) and the diaphragm (right) when implanted in muscle as a function of diameter and aspect ratio.

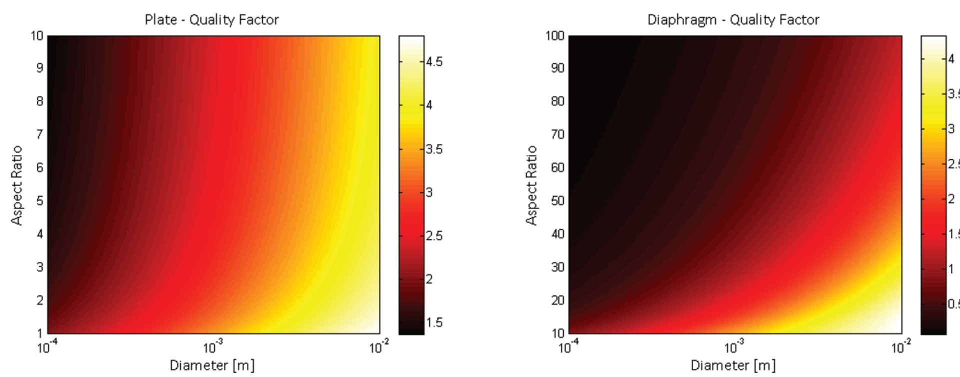

Figure 9. Combined quality factor (acoustic radiation loss, viscous drag, and manufacturer-specified "Mechanical Q") for the plate (left) and the diaphragm (right) when implanted in muscle as a function of diameter and aspect ratio.

Piezoelectric coupling

The piezoelectric coupling coefficient, k^2, is a value between 0 and 1 and is defined as the mechanical/electrical energy converted to electrical/mechanical energy divided by the total input mechanical/electrical energy. The value of the coupling coefficient varies according to material and the direction of strain relative to the direction of polarization. The plate architecture operates in the 3-3 mode meaning strain and polarization are in the same direction resulting in a high coupling coefficient. Piezo manufacturers typically specify k_{33} and k_t. Both values refer to the 3-3 mode but k_{33} is for cylinders (aspect ratio $\ll 1$) and k_t is for plates (aspect ratio ≥ 1) and k_t is typically lower than k_{33}. On the other hand, the diaphragm operates in the 3-1 mode meaning that strain and polarization are perpendicular to each other resulting in a lower coupling coefficient. The value k_{31} refers to the 3-1 mode and is typically lower than both k_{33} and k_t (see Table 2). For PZT, the 3-3 coupling coefficient is approximately four times larger than the 3-1 coupling coefficient. Note, this does not mean that the 3-3 mode is four times more efficient. It means that more of the mechanical excitation energy is converted to electrical energy. The unconverted mechanical energy is not necessarily lost. Much of it will be retained as kinetic energy in the plate or diaphragm. In general, more highly coupled systems are able to generate more power. However, there is a point of diminishing returns where extra coupling serves to further dampen the system reducing mechanical displacements and the power conversion becomes self-limiting in a way. The point at which extra coupling is no longer of much benefit depends on the mechanical quality factor (Q_{tot}). If the quality factor is higher, high output power will be achieved with lower piezoelectric coupling. If the quality factor is lower, high output power will require higher levels of piezoelectric coupling.

It is important to note that the magnitude of the power transduced is proportional to the volume of the piezoelectric material and proportional to the square of the average strain induced in the material. Since diaphragms typically utilize significantly less piezoelectric material than plates of the same diameter, diaphragms are disadvantaged. However, this disadvantage is mitigated by the fact that their strain level is generally much higher than plates. The effect of piezoelectric coupling

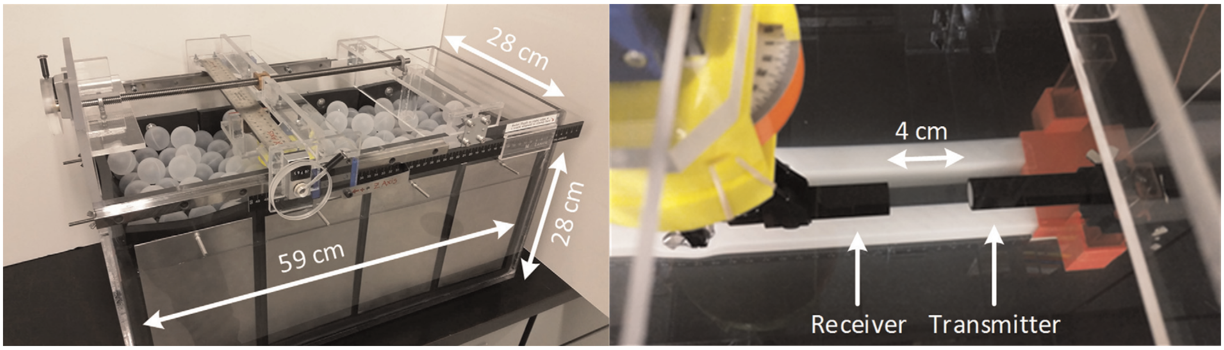

Figure 10. Left: acoustic test tank with absorber panels and positioning system. Right: plate transmitter and receiver separated by water in the acoustic test tank.

is embedded in the plate and diaphragm equivalent circuit models.

Power electronics

Power electronics, whether passive or active, will be required to condition the power in order to be compatible with sensors and other devices. To simplify the comparison between the plate and diaphragm architectures, power electronics will not be considered in this article. However, a comparison of power electronics for piezoelectric energy harvesters can be found in Guyomar and Lallart (2011).

Electrical impedance mismatch

Electrical impedance mismatch is similar to acoustic pressure wave reflection where the electrical power is reflected instead of acoustic power and the mismatch is between the electrical load impedance and the electrical impedance of the piezo. With ultrasonic transducers, electrical matching is often called tuning. Tuning a transducer involves adding an inductor (and resistor) in parallel with the piezoelectric capacitance, C_0, to match the electrical resonance to the mechanical resonance. This can be done for both the plate and the diaphragm transducers to significantly increase the power generated. However, depending on the size and mechanical resonance frequency of the transducer, it may not be practical to fit the required inductor on an implant. For this reason, full complex matching (inductor plus resistor) is replaced by resistive matching (resistor with value of $1/\omega C_0$), shown in Figure 3, for simplification.

Experimental setup and model validation

To validate the plate and diaphragm equivalent circuits paired with the loss relationships discussed previously, the experimental data were obtained from macro-scale devices and compared to simulation data. To obtain the experimental data, a $59 \times 28 \times 28$ cm^3 tank with acoustic absorbers and transducers, shown in Figure 10, was constructed. The acoustic absorber panels were fabricated from 12.7-mm-thick ultra-soft polyurethane (McMaster Carr; 8514K75) which experimentally exhibits a fairly steady 90.6% pressure attenuation after one pass between 5 kHz and 1.25 MHz. For the transducers, piezoelectric plates (APC Inc.; 851 material, 1.9 mm thick, 12.8 mm diameter) and diaphragms (Steminc; SMPD11D11T10F95) were mounted to ABS tubing (McMaster Carr; 1839T371) with cyanoacrylate and placed in the distilled water–filled tank as transmitter–receiver pairs. Tests were run with a swept 2.5 V_{pk} sinusoidal input from a function generator (Rigol DG1022A) connected to a power amplifier (Rigol PA1011) in series with a 100 ohm resistor. Data were collected using a spectrum analyzer (PicoScope 2206) on peak-hold mode. Frequency sweep ranges were between 950 kHz and 1.15 MHz for the plate transducers and between 2.5 and 4.5 kHz for the diaphragm transducers over 120 s. During the test, the receiver load current was measured and recorded. It should be noted that although the frequency range of the diaphragm is not in the ultrasonic region (above 20 kHz) and the 100 ohm load resistor is not the optimal load resistor value for the transducers, the experiment still serves the end goal of validating the network equivalent models of the transducers. The resistor values and transducers were chosen to facilitate manufacturing and testing.

Simulations were performed using the models shown in Figure 11 and the material properties given in Table 3 and are compared with the measured receiver load current shown in Figure 12. The simulated results are in close agreement with the experimental data. A few important notes about Figure 12 should be considered: (1) beam divergence for the diaphragm is approximated by assuming a divergence angle of 90° which translates to the effective beam radius, r_{beam}, being equal to the separation distance between the diaphragms. In the following section, beam divergence will be neglected to simplify the analysis and provide more insightful results. (2) Only analytical relationships, not

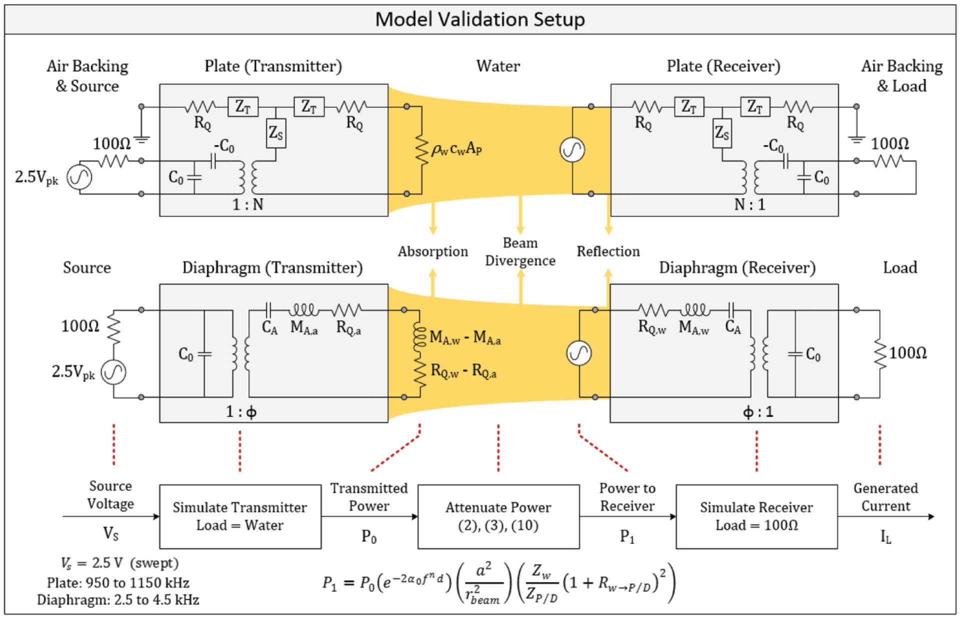

Figure 11. Network model used to validate the plate and diaphragm equivalent circuit models coupled with loss relationships for the plate (top) and the diaphragm (bottom). The transmitter acoustic power output is modeled as the power dissipated across the impedance in the "Water" area of the diagram. The receiver source is modeled as the transmitter acoustic power output minus absorption, beam divergence, and reflection losses.

Table 3. Properties (left) and millimeter dimensions (right) of the plates and diaphragms used for model validation.

Variable		Plate APC 851	Diaphragm piezo NAVY-II	Diaphragm shim Brass	Units
Density	ρ	7600	7600	10,490	kg/m^3
Speed of sound	c	4080 + 3%	4080	3650	m/s
Young's modulus	Y_{31}	63	63	100	GPa
	Y_{33}	54	54		
Poisson's ratio	ν	0.32	0.32	0.32	–
Permittivity	ε	17.258	16.815		nF/m
Charge constant	d_{31}		−0.175		nm/V
	d_{33}	0.4			
Coupling coefficient	k_{31}		0.36		–
	k_t	0.51			

Sources: APC International, Ltd (2013), Engineering ToolBox (2015a),(2015b).

empirical measurements, are used to obtain the quality factor used in the simulation model. In the following section, the same analytical relationships will be used to obtain simulation results as the transducers are scaled down in size. (3) The experimental data for the plate exhibit peaks that are not accounted for by the simulation. These peaks are standing waves and are a result of the dynamics of the medium between the transmitter and the receiver. The frequencies at which the standing waves appear are given in equation (17). The amplitude of the peaks is dependent on transmitter diameter, frequency, transmitting depth, and medium material properties and is an important consideration when designing a full transmitter–medium–receiver system. Since the focus of this article is the comparison of receiver architectures, the medium dynamics are neglected in all simulation data in this article. In this section, neglecting the medium dynamics and including the transmitter dynamics provides a comparison between the simulation model and experimental data with a preliminary feel for the power variation the receiver can experience as the transmitter frequency is slightly altered (see Table 4). In the following section, neglecting the medium and transmitter dynamics provides a cleaner visual comparison between receiver architectures with generated power values isolated from transmitter and medium resonances

$$f_{\text{standing waves}} = \frac{nc_w}{2d} \qquad n = 1, 2, 3, \ldots \tag{17}$$

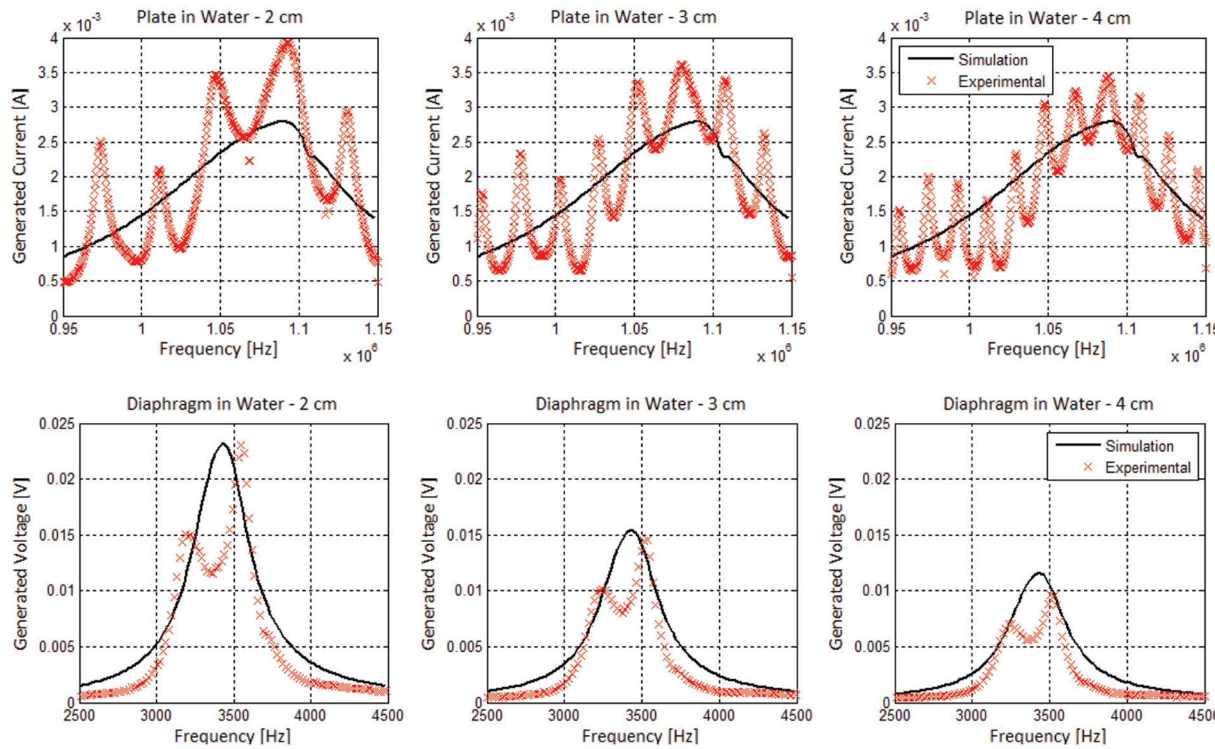

Figure 12. Experimental (red x) and simulation (black line) data for the transmitter–receiver model validation setup at 2, 3, and 4 cm separation distances in water for the plate (top) and diaphragm (bottom).

Table 4. Characteristics of standing waves shown in experimental plate data in Figure 12.

Depth (cm)	Approx. standing wave amplitude (mA)	Repeats every … (kHz)
2	0.8837	39.9
3	0.7866	24.6
4	0.6340	18.6

Generated power comparison

Scaling simulations were performed to compare the load power generated by the plate to that of the diaphragm as diameter is swept from centimeter to submillimeter sizes. The circuit configuration used for the scaling simulations, shown in Figure 3 (right), has an intensity source of 7200 W/m^2 and assumes zero beam divergence. The material properties used for the simulations are given in Table 2. The following paragraphs compare the load power of the plate and diaphragm in terms of diameter, aspect ratio, and tissue depth.

Aspect ratio and diameter

Figure 13 shows the load power generated by the plate and diaphragm embedded 2 cm into the muscle as a function of aspect ratio and diameter. It should be noted that the load power was evaluated at the resonance frequency of the loaded transducer, not necessarily at the optimal load power point. The figure reveals that higher load power for the plate tends to occur at larger diameters and smaller aspect ratios while higher load power for the diaphragm generally increases with diameter but is less sensitive to aspect ratio. It also shows that the plate load power decreases more rapidly with decreasing diameter than the diaphragm load power because the plate operates at higher frequencies and thus suffers from higher tissue absorption. When designing a small ultrasonic implant, the aspect ratio of the plate and the resonance frequency of the diaphragm may become constraints. For the plate, a small aspect ratio means higher load power, but also means a thicker transducer that may not fit on the implant (an aspect ratio of 1 means that the diameter and thickness are the same size) or even be manufacturable. For the diaphragm, lower resonance frequencies are desirable because they result in lower absorption. However, if the transducer is to be an ultrasonic transducer, then the resonance frequency cannot be lower than 20 kHz. It is important to consider that cavitation becomes more of a concern at high pressures and low frequencies.

To reduce the risk of cavitation, the US FDA has set a mechanical index limit, MI given in equation (18), of 1.9 (0.23 for ophthalmic) (Guidance for Industry and FDA Staff Information for Manufacturers Seeking Marketing Clearance of Diagnostic Ultrasound

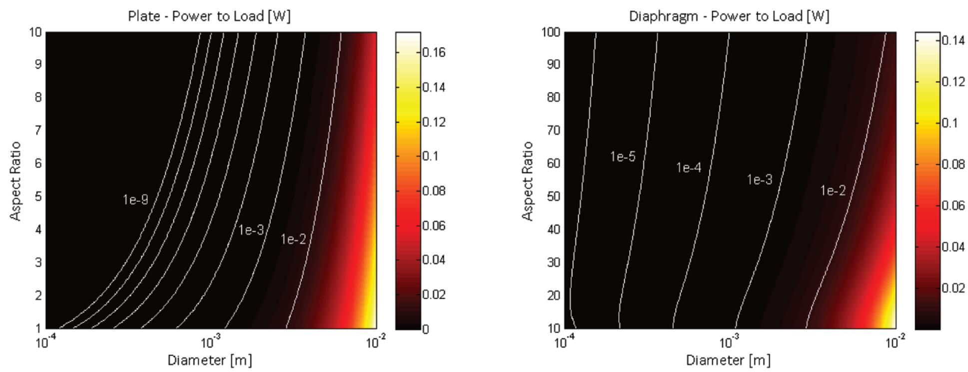

Figure 13. Receiver load power for the plate (left) and the diaphragm (right) when implanted 2 cm deep into muscle with a source intensity of 7200 W/m^2. Each white contour line represents an order of magnitude decrease.

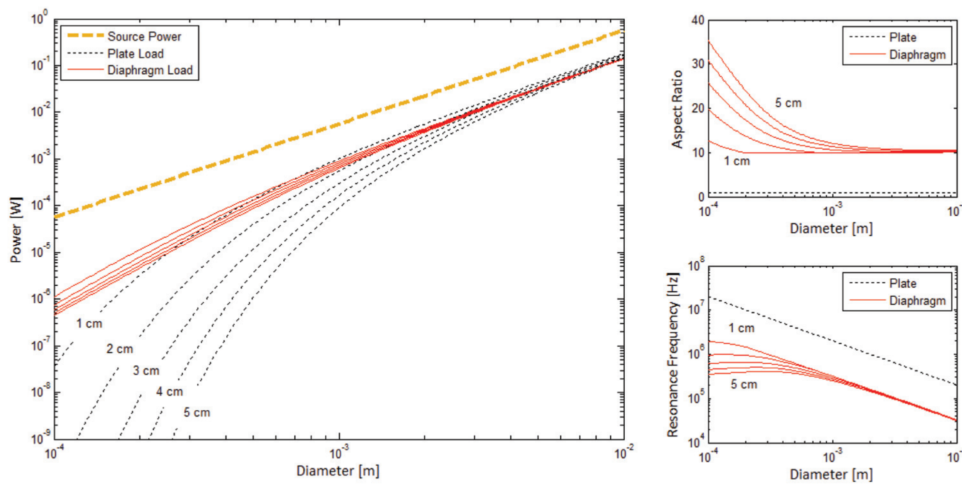

Figure 14. Left: power delivered to the implant's load at 1, 2, 3, 4, and 5 cm depths for the untuned plate and diaphragm without matching layers. Right-top: aspect ratio required. Note that 1 cm depth corresponds to the top diaphragm line and 5 cm depth corresponds to the bottom diaphragm line.

Systems and Transducers, 2008). Let us consider the case referred to in this article that is most vulnerable to cavitation (e.g. 20 kHz, 7200 W/m^2, 1.675 MRayl). In this case, the pressure in the muscle ($p = \sqrt{IZ_{\text{muscle}}}$) is 0.109839 MPa. At 20 kHz, MI is 0.776, which is well below the 1.9 limit

$$MI = \frac{\text{Negative Peak Pressure in MPa}}{\sqrt{\text{Frequency in MHz}}} \tag{18}$$

Depth and diameter

Figure 14 shows the load power generated by the plate and diaphragm as a function of diameter at various implant depths in muscle. The most important feature of Figure 14 is the load power comparison between the plate and diaphragm. In terms of power generated, the plate and diaphragm are comparable in the range between 1 mm and 1 cm. In this range, design factors other than power, such as quality factor, operating pressure, generated voltage, and thickness constraints, would determine which architecture to use. Below 1 mm, the diaphragm becomes a far more enticing choice for power generation because its generated power is much less sensitive to implant depth than that of the plate and the overall power generated is greater. A few important points should be noted: (1) Figure 14 shows the optimal transducer design for each diameter and depth combination. For the plate, the optimal design happens to be a transducer with aspect ratio of 1 for all depths and diameters. For the diaphragm, the optimal design occurs at a different aspect ratio for each diameter and depth because there is a significant trade-off between frequency (tissue absorption) and the piezo volume (generating potential). (2) Below 1 mm, the plate load power degrades significantly with implant depth because its resonance frequency is very high.

Conclusion

This article has analyzed two piezoelectric power generator architectures for an acoustic power transmission system intended to provide power to small, deeply implanted bio-devices. Specifically, this article has compared the power loss mechanisms and total power generated for the plate and diaphragm (i.e. PMUT) architectures in terms of diameter, aspect ratio, and implanted depth. Simulation results showed that for implants in muscle, the plate and diaphragm generate a comparable amount of power for generator diameters in the millimeter range. For generator diameters in the sub-millimeter range, the diaphragm generally generates more power than the plate and is significantly less sensitive to changes in implant depth.

Declaration of conflicting interests

The authors declared no potential conflicts of interest with respect to the research, authorship, and/or publication of this article.

Funding

The authors gratefully acknowledge funding for this work from the National Science Foundation under Award Number ECCS 1408265.

References

APC International, Ltd (2013) *Physical and piezoelectric properties of APC materials*. Available at: https://www.americanpiezo.com/apc-materials/physical-piezoelectric-properties.html (accessed January 2015).

Arra S, Leskinen J, Heikkilä J, et al. (2007) Ultrasonic power and data link for wireless implantable applications. In: *International Symposium on Wireless Pervasive Computing*, San Juan, 5–7 February, pp. 567–571.

Christensen DA (1988) *Ultrasonic Bioinstrumentation*. USA: John Wiley & Sons, Ltd.

Denisov A and Yeatman E (2010) Ultrasonic vs. inductive power delivery for miniature biomedical implants. In: *2010 international conference on body sensor networks (BSN 2010)*, pp. 84–89. Available at: http://ieeexplore.ieee.org/lpdocs/epic03/wrapper.htm?arnumber=5504736

Engineering ToolBox (2015a) Speed of sound in some common solids. Available at: http://www.engineeringtoolbox.com/sound-speed-solids-d_713.html (accessed January 2015).

Engineering ToolBox (2015b) Tensile modulus—modulus of elasticity or Young's modulus—for some common materials. Available at: http://www.engineeringtoolbox.com/young-modulus-d_417.html (accessed January 2015).

Fox R, Pritchard P and McDonald A (2009) *Introduction to Fluid Mechanics*. 7th ed. Hoboken, NJ: John Wiley & Sons, Ltd.

Guidance for Industry and FDA Staff Information for Manufacturers Seeking Marketing Clearance of Diagnostic Ultrasound Systems and Transducers (2008) Center for Devices and Radiological Health, Food and Drug Administration, US Department of Health and Human Services.

Guyomar D and Lallart M (2011) Recent progress in piezoelectric conversion and energy harvesting using nonlinear electronic interfaces and issues in small scale implementation. *Micromachines* 2(4): 274–294. Available at: http://www.mdpi.com/2072-666X/2/2/274/ (accessed 11 April 2014).

Jacobitz F, Anderson S and Babila E (2011) A comparison of the microcirculation in rat spinotrapezius muscle and muscle fascia. Available at: http://documents.irevues.inist.fr/handle/2042/36675 (accessed January 2015).

Kawanabe H, Katane T, Saotome H, et al. (2001) Power and information transmission to implanted medical device using ultrasonic. *Japanese Journal of Applied Physics* 40(5): 3865–3866.

Kim S, Clark WW and Wang Q (2003) Piezoelectric energy harvesting using a diaphragm structure. *Smart Structures and Materials* 5055: 307–318.

Kozlovsky Y (2009) Vibration of plates in contact with viscous fluid: extension of Lamb's model. *Journal of Sound and Vibration* 326(1–2): 332–339. Available at: http://linkinghub.elsevier.com/retrieve/pii/S0022460X09003538 (accessed 14 April 2014).

Lamb H (1920) On the vibrations of an elastic plate in contact with water. *Proceedings of the Royal Society A: Mathematical, Physical and Engineering Sciences* 98(690): 205–216. Available at: http://rspa.royalsocietypublishing.org/cgi/doi/10.1098/rspa.1920.0064 (accessed 21 April 2014).

Mo C, Radziemski LJ and Clark WW (2010a) Analysis of piezoelectric circular diaphragm energy harvesters for use in a pressure fluctuating system. *Smart Materials and Structures* 19(2): 025016. Available at: http://stacks.iop.org/0964-1726/19/i=2/a=025016?key=crossref.f4d118d36a50a04f8b6248cf83bf8021 (accessed 17 March 2014).

Mo C, Radziemski LJ and Clark WW (2010b) Experimental validation of energy harvesting performance for pressure-loaded piezoelectric circular diaphragms. *Smart Materials and Structures* 19(7): 075010. Available at: http://stacks.iop.org/0964-1726/19/i=7/a=075010?key=crossref.6411b2bfd2bf4bce80c16b0098495723 (accessed 17 March 2014).

Olfatnia M, Shen Z, Miao JM, et al. (2011) Medium damping influences on the resonant frequency and quality factor of piezoelectric circular microdiaphragm sensors. *Journal of Micromechanics and Microengineering* 21(4): 045002. Available at: http://stacks.iop.org/0960-1317/21/i=4/a=045002?key=crossref.d61a2f265523ab76a5ece2ae30f589c6 (accessed 14 April 2014).

Ozeri S and Shmilovitz D (2010) *Ultrasonic transcutaneous energy transfer for powering implanted devices*. *Ultrasonics* 50(6): 556–566. Available at: http://www.ncbi.nlm.nih.gov/pubmed/20031183 (accessed 15 June 2013).

Prasad SAN, Gallas Q, Horowitz SB, et al. (2006) Analytical electroacoustic model of a piezoelectric composite circular plate. *AIAA Journal* 44(10): 2311–2318. Available at:

&http://arc.aiaa.org/doi/abs/10.2514/1.19855 (accessed 5 June 2013).

Ramsay MJ and Clark WW (2001) Piezoelectric energy harvesting for bio-MEMS applications. In: *Smart materials and structures*, vol. 4332 (ed A-MR McGowan), pp. 429–438. Available at: http://proceedings.spiedigitallibrary.org/proceeding.aspx?articleid = 908216

Sanni A, Vilches A and Toumazou C (2012) Inductive and ultrasonic multi-tier interface for low-power, deeply implantable medical devices. *IEEE Transactions on Biomedical Circuits and Systems* 6(4): 297–308. Available at: http://www.ncbi.nlm.nih.gov/pubmed/23853174

Seo D, Carmena JM, Rabaey JM, et al. (2013) *Neural dust: an ultrasonic, low power solution for chronic brain-machine interfaces*. April, arXiv:1307.2196 [q-bio.NC].

Sherrit S, Leary SP, Dolgin BP, et al. (1999) Comparison of the Mason and KLM equivalent circuits for piezoelectric resonators in the thickness mode. In: *1999 Proceedings of IEEE ultrasonics symposium*, vol. 2 (Cat. no.99CH37027), pp. 921–926. Available at: http://ieeexplore.ieee.org/lpdocs/epic 03/wrapper.htm?arnumber = 849139

Sherrit S, Badescu M, Bao X, et al. (2005) Efficient electromechanical network models for wireless acoustic-electric feedthroughs. In: *Proceedings of the SPIE smart structures conference*, San Diego, CA, 6–10 March.

Shigeta Y, Hori Y, Fujimori K, et al. (2011) Development of highly efficient transducer for wireless power transmission system by ultrasonic. In: *2011 IEEE MTT-S international microwave workshop series on innovative wireless power transmission: technologies, systems, and applications*, pp. 171–174. Available at: http://ieeexplore.ieee.org/articleDetails.jsp?arnumber = 5877115&;contentType = Conference + Publications (accessed 15 December 2012).

Smyth KM (2012) *Design and Modeling of a PZT Thin Film Based Piezoelectric Micromachined Ultrasonic Transducer (PMUT)*. Cambridge, MA: Massachusetts Institute of Technology.